

Discovery of Nb hydride precipitates in superconducting qubits

Jaeyel Lee^{1*}, Zuhawn Sung^{1*}, Akshay A. Murthy¹, Matthew J. Reagor², Anna Grassellino¹, and Alexander Romanenko^{1†}

¹Fermi National Accelerator Laboratory (FNAL), Batavia, IL 60510, USA

²Rigetti Computing, 2919 Seventh Street, Berkeley, CA 94710, USA

Abstract

We report the first evidence of the formation of niobium hydrides within niobium films on silicon substrates in superconducting qubits fabricated at Rigetti Computing. We combine complementary techniques including room and cryogenic temperature atomic scale high-resolution and scanning transmission electron microscopy (HR-TEM and STEM), atomic force microscopy (AFM), and the time-of-flight secondary ion mass spectroscopy (TOF-SIMS) to reveal the existence of the niobium hydride precipitates directly in the Rigetti chip areas. Electron diffraction and high-resolution transmission electron microscopy (HR-TEM) analyses are performed at room and cryogenic temperatures (~ 106 K) on superconducting qubit niobium film areas, and reveal the formation of three types of Nb hydride domains with different crystalline orientations and atomic structures. There is also variation in their size and morphology from small (~ 5 nm) irregular shape domains within the Nb grains to large (~ 10 -100 nm) Nb grains fully converted to niobium hydride. As niobium hydrides are non-superconducting and can easily change in size and location upon different cooldowns to cryogenic temperatures, our findings highlight a new previously unknown source of decoherence in superconducting qubits, contributing to both quasiparticle and two-level system (TLS) losses, and offering a potential explanation for qubit performance changes upon cooldowns. A pathway to mitigate the formation of the Nb hydrides for superconducting qubit applications is also discussed.

*These authors contributed equally

[†] Corresponding author: aroman@fnal.gov

Introduction

Niobium thin films of ~100-200 nm thickness are key components of a superconducting qubit architecture for quantum computing applications, as they are used to pattern the readout resonators, coupling lines, and the capacitance pads of the qubits [1, 2]. Any microwave dissipation mechanisms present in these niobium films are therefore primary contributors to the decoherence of the superconducting qubits. There have been intensive studies to understand the microscopic origins of the decoherence in the superconducting qubits [1, 3], and several coherence-limiting mechanisms have been identified. These include two-level systems (TLS) hosted by amorphous oxides at various interfaces [1, 4], i.e. metal-air [5-7, 11], metal-substrate [8-10], and substrate-air interfaces [5, 9], which have been recently shown to be the primary coherence-limiting mechanism in the quantum regime for 3D superconducting radio frequency (SRF) cavities [11]. Additionally, non-equilibrium quasiparticles [30], including those produced by the cosmic rays and environmental radioactivity [31, 32] are considered as another possible decoherence mechanism.

It has been previously discovered in bulk niobium SRF cavities [34, 25, 29, 16] that the formation of the non-superconducting niobium nano-hydrides upon cooldown from room temperature to cryogenic temperatures ($< \sim 150\text{K}$) introduces a major dissipation mechanism, which limits achievable quality factors [29]. This is due to the fact that Nb can adsorb a significant amount of hydrogen (H) even at room temperature - whenever it is not passivated by a layer of native niobium oxide (Nb_2O_5) - which then can easily form Nb hydride compounds at suitable temperatures and concentrations [12, 13]. Hydrogen atoms can sit on 12 tetrahedral sites of a BCC Nb lattice, and depending on H concentration, can form a variety of different Nb hydrides in the Nb matrix [12]. The additional microwave dissipation emerges due to Nb hydrides being poor or non-superconductors [14], gaining superconductivity only by the proximity effect within the superconducting niobium matrix [29]. The possible presence and dissipation due to niobium hydrides, well-studied in bulk niobium SRF cavities, has not been so far considered for the 2D superconducting qubits.

In this study, we apply the same methodology used to reveal the niobium hydrides in bulk SRF cavities, to niobium film parts of the full superconducting qubit chips from Rigetti Computing. We combine the room and cryogenic temperature atomic force microscopy (AFM), atomic scale high-resolution and scanning transmission electron microscopy (HR-TEM and STEM) on focused ion beam (FIB) prepared lamellae, and the time-of-flight secondary ion mass spectroscopy (TOF-SIMS) to reveal the existence of the niobium hydrides directly in the Rigetti chip parts. Further detailed investigations to suppress the formation of the Nb hydrides are underway.

Experimental procedure

Superconducting qubit devices with Nb resonators and $\text{Al}/\text{AlO}_x/\text{Al}$ Josephson junctions have been fabricated on a Si (100) substrate at Rigetti Computing based on the optimized nanofabrication procedure [15]. The chip containing five superconducting qubits, readout resonators, and connecting lines has been used for the studies.

To search for niobium hydride formation, several complementary approaches were used. Firstly, to study the internal niobium structure throughout the films, focused ion beam has been used to prepare several TEM lamellae for subsequent room and cryogenic temperatures studies. Electron diffraction has been used to search for and confirm the presence of niobium hydride phases in the niobium matrix.

Secondly, the atomic force microscopy (AFM) using the attoCube system has been performed directly looking at various areas of the superconducting qubit chip at temperatures from room temperature down to about 2 K. AFM allows a plan view of about 18x18 μm to be observed throughout the changing temperatures to search for morphological changes on the surface caused by the niobium hydride formation, similar to [34, 25, 40].

Scanning electron microscopy (SEM) imaging of the superconducting qubit and TEM sample preparation were carried out with Helios Nanolab 650. TEM lamellae were prepared using 30 kV Ga ion beam and finely polished by 5 kV and 2 kV Ga ion beams in order to obtain high electron transparent imaging as well as to remove the damaged surface on the Nb foils. Annular dark-field scanning transmission electron microscopy (ADF-STEM) and HR-TEM were performed on JEOL ARM200CF electron microscope operated at 200 kV. The microscope was equipped with a Cold FEG source and probe aberration corrector. ADF images were acquired using a convergence semi-angle of 21 mrad and collection angles of 68-260 mrad. Gatan LN₂ single-tilt TEM cold stage was used to cool the foils down to cryogenic temperature (106 K), which is confirmed to be sufficient for β , ϵ , λ NbH phase [16].

To provide further insight into the origin of the niobium hydride emergence, we have used a dual beam time-of-flight secondary ion mass spectrometry (TOF-SIMS) – IONTOF 5 - to analyze the concentration and depth distribution of hydrogen in Nb parts of the chip. Secondary ion measurements were performed using a liquid bismuth ion beam (Bi⁺) and a cesium ion gun with an energy of 500 eV was used for sputtering the surface for depth profile measurements.

Experimental results

In **Fig. 1(a)** the schematic of the Si substrate with the Al/AlO_x/Al Josephson junction area and Nb film pads is shown. Morphology of the surface of Nb films is analyzed using AFM at room and cryogenic temperatures, as shown in **Fig. 1 (b-e)**. At room temperature (RT), the surface of Nb is smooth, displaying root-mean-square (RMS) roughness values < 1 nm. However, we observe two distinct changes of surface morphology during cooling down to 2 K. Firstly, irregularly shaped structures of ~500 nm lateral diameter and 10-20 nm of height appear on the surface of the Nb films as the temperature approaches 200 K and persist throughout the cooldown to 5 K, as shown in **Fig. 1 (b,c)**. Additional topographical features with the size of the order of ~2 nm are observed to emerge in some of the Nb grains as well, **Fig. 1 (d,e)**. In the case of bulk Nb SRF cavities, similar surface features have been previously detected at cryogenic temperatures and have been shown to result from the precipitation of Nb hydrides [25, 40].

Annular dark-field (ADF)-STEM image in **Fig. 2(a)** displays the cross-section of the Nb film on Si. From secondary ion-mass spectroscopy (SIMS) depth profile measurements directly performed on several Nb resonator regions from the same qubit device, we detect an appreciable level of hydrogen at the surface, **Fig. 2(b)**. We find that the H-/Nb signal, which represents a measure of the free hydrogen concentration present in the parent Nb matrix, is high right underneath the niobium oxide, and then decays to a much lower level within first ~10 nm from the surface. The presence of this hydrogen at the surface corroborates with previous findings in bulk Nb cavities and enables the possibility of the Nb hydride formation in Nb thin film geometries as well. In addition to hydrogen, a significant concentration of other impurities is observed – examples of the observed O-/Nb and C-/Nb signals, which are also decaying on a larger scale than the H-/Nb signal, are shown in **Fig. 2(b)**.

To further confirm the presence of Nb hydrides in Nb grains within the superconducting coplanar resonators, TEM analysis is performed at room and cryogenic temperatures (106 K). Seven TEM samples and the total of 450 ± 50 Nb grains have been analyzed. In the case of room temperature (RT) measurements,

we observed three types of Nb hydride structures differing by their orientation in the Nb films on Si substrates. There are also variations in morphology and size of the hydrides, ranging from small size (~3-5 nm) irregular shape domains to distinct shape large (~10-100 nm) Nb hydride domains with sharp Nb/Nb hydride interfaces.

The structure of Nb hydrides is analyzed in detail using HR-TEM and electron diffraction and they exhibit different orientations of the hydrogen in the Nb matrix, **Figs. 3-5**. These observed diffraction patterns agree with the orientations of Nb hydride atomic arrangements summarized in **Fig. 5**.

Firstly, we assert that “Type I” Nb hydrides correspond to the situation where the (100) plane of orthorhombic ϵ -NbH_x is parallel to the Nb (110) plane in the film, which is surface normal direction. HR-TEM image of the small Nb hydride domain is shown in **Fig. 3**. A nano-beam electron diffraction pattern is taken on grain no. 6 in **Fig. 2(a)**, and it reveals the additional reflections, which are from the Nb hydride domain in the Nb grain, **Fig. 3(a)**. FFT of the region with Nb hydride also matches the diffraction pattern of ϵ -Nb hydride on bcc Nb [111] zone axis [12]. Inverse FFT of the additional reflection reveals the distribution of ~5 nm scale Nb hydride domain in the Nb grain. In some cases, they have a small size (3-5 nm) with irregular shapes and, they also occupy whole Nb grain with possibly causing significant lattice distortion. Some of the small Nb hydride precipitates are seen at GBs, suggesting that GBs could be among the preferential hydride nucleation sites.

Secondly, FFT of the HR-TEM image from another Nb grain shows that (100) plane of orthorhombic ϵ -NbH_x is parallel to another Nb (011) or (1 $\bar{1}$ 0) planes which are 60° off from the surface normal (110) plane (“Type II”). For the second case, large sizes (10-100 nm) of Nb hydride domains are observed with distinct shapes. **Fig. 5** shows the HR-TEM image of a Type II Nb hydride domain embedded in the Nb matrix, with ~20 nm width and ~100 nm length along the depth direction of the Nb film. Based on the HR-TEM image of the Nb hydride domain, we find that for this type of hydride, the (100) plane of ϵ -NbH_x is parallel to (1 $\bar{1}$ 0) planes, which is 60° off from Nb (110), the surface normal plane of the Nb film. HR-TEM image displays that they form sharp interfaces with the Nb matrix along the {110} planes, which is the slip plane of BCC Nb.

Lastly, another type of Nb hydride domain is also observed. **Fig. 6(a,b)** displays the HR-TEM image of the Nb grain on the [131] zone axis with two Nb hydride domains. Inset in **Fig. 6(b)** is FFT of the HR-TEM image of the Nb grain, indicating the additional reflection from the two Nb hydride domains. Nano-beam electron diffraction is taken on the Nb grain on the [131] zone axis with one of the two hydride domains, **Fig. 6(c)**, and demonstrate that additional reflection appear from possible hydride formation. To identify the phase of the Nb hydride domain 1 and 2 in the Nb grain, electron diffraction simulation is performed using CaRine Crystallography software (version 3.1) [17], and details are described in the supplementary information, **Fig. S1**. We also note that the Nb/Nb hydride domain interfaces are formed along the Nb {112} plane, which is another slip plane of BCC Nb.

Next, we employed cryo-TEM analyses to find the changes of Nb hydride at cryogenic temperatures as indicated in the cryo-AFM experiments, **Fig.1**. The change of the eight grains in the ADF-STEM image of **Fig. 2(a)**, from grain no. 0 to no. 7, are selected for detailed analyses. For the small Nb hydride domain in grain no. 1 and 6, they are still observed in the electron diffraction pattern but significant additional nucleation of Nb hydride domains is not observed. For the large distinct Nb hydride domains in grain no. 7, **Fig. 6**, they still maintain their shape and there are no significant changes in their size within ~5 nm. For other Nb grains which do not have Nb hydride domains at RT (grain no. 0, 2, 3, 4, and 5), nucleation of Nb hydride domain is not observed at 106 K and they still maintain bcc Nb structures. It is possible that additional formation of small Nb hydride domains (3-5 nm) or growth of distinct shaped Nb hydride domain

along with the Nb/Nb hydride interface take places in other regions but they are not easily noticed in the cryo-TEM due to the complex contrast and reduced resolution at cryogenic temperatures, **Fig. S2**. Additional AFM and X-ray diffraction (XRD) at cryogenic temperatures are planned to clarify the change of structures of Nb hydrides in Nb films in the superconducting qubits.

Discussion

Our results indicate the Nb hydride formation in Nb films of superconducting qubits, with hydrides present even at room temperature. This is a significant difference from the bulk Nb SRF cavities, where hydride formation has so far been observed when going to cryogenic temperatures [25, 16]. TEM analyses indicate that the volume fraction of Nb hydrides in the Nb films of investigated superconducting qubit chips is roughly estimated to be 0.1~1%.

Oxygen, nitrogen and other impurities serve as effective hydrogen trapping centers [26, 27], and prevent formation of the large hydrides [25] responsible for the “hydrogen Q disease” in low RRR bulk niobium SRF cavities [28]. Similarly, oxygen diffusion and the resulting hydrogen trapping are behind the 120C baking effect eliminating the nanohydrides and the high field Q-slope in high RRR SRF cavities [27]. Considering the low residual resistance ratio (RRR) values of sputtered Nb films we studied [5, 33], and high concentrations of non-hydrogen impurities confirmed by our TOF-SIMS results, the formation of the Nb hydrides in Nb film parts of the qubit chip is quite surprising. One possible explanation is the much larger concentration of crystalline defects – eg dislocations, vacancies, grain boundaries - in the films as compared to bulk niobium in SRF cavities. This can both make the hydrogen distribution highly non-uniform, enabling local higher concentration areas, and provide plenty of hydride nucleation sites to facilitate the precipitation. Further investigations into this aspect and detailed comparisons with the well-studied bulk niobium are ongoing and will be reported in future publications.

There are several possibilities for the causes of the hydrogen loading and subsequent hydride formation in the qubit Nb films. Firstly, hydrogen atoms may be incorporated during the coating process due to residual hydrogen in the sputtering chamber. Furthermore, as studied in detail for bulk niobium, any chemical [35], annealing [36-38], or mechanical polishing [39] steps in the manufacturing process, which eliminate the protective Nb₂O₅ layer on top of Nb, can lead to hydrogen loading, if the processes are performed in the hydrogen-containing environment. Further investigations to pinpoint such fabrication steps dominating the hydrogen incorporation into niobium films are currently underway.

We have also investigated the possible effect of Ga ion beam on the formation of hydrides in Nb during the sample preparation process using bulk Nb samples. There have been reports that Ga ion beam introduces hydrogen and large distinct shaped hydride phases could form in Ti [19] and Zr [20] during the TEM sample preparation using FIB. However, Ti and Zr have a higher affinity to hydrogen than Nb and we could not observe hydride formation in the TEM foils of bulk Nb after TEM sample preparation using FIB with the same parameters. Therefore, we conclude that Ga ion beam effect is not significant in Nb foils and Nb hydride phases we observed in the current study are formed during or after the film growth or subsequent chip patterning and fabrication process.

It is important to note that the hydride structure could change upon subsequent cooldowns, as studied in detail in bulk Nb [25]. This can provide a potential explanation for the observed qubit coherence time changes in different cooldowns, as well as the effect of “aging” from the accumulated number of cooldowns.

There could be a couple of strategies to mitigate the formation of Nb hydride domains in Nb films. Similarly to SRF Nb cavities, post-annealing of Nb film at above around 600C may degas hydrogen atoms from Nb, and reduce the formation of Nb hydride domains [21, 22]. One potential challenge is that at such higher temperatures, Nb silicide can be formed at the Nb/Si interfaces, thus using a sapphire substrate instead may enable a more suitable temperature range of heat treatments. The structure of GBs may also play a role in the formation of Nb hydrides near GBs of Nb [23, 24]. Further optimization of the microstructure of Nb films such as grain size, texture, and the structure of grain boundaries may provide an additional pathway to mitigate the hydride formation and suppress the hydride-induced decoherence in Nb superconducting planar resonators and superconducting qubits. Such an optimization may be performed by exploring various state-of-the-art niobium film deposition techniques, including those leading to much higher RRR values, a subject of another ongoing investigation to be reported in our future publications.

Conclusion

We report the discovery of the non-superconducting Nb hydride domains in Nb films of state-of-the-art superconducting qubit chips, as revealed by a combination of the transmission electron microscopy (TEM), atomic force microscope (AFM), and secondary ion mass spectrometry (SIMS). High-resolution TEM imaging and electron diffraction of Nb films indicate that Nb hydride domains exist in the Nb film parts of superconducting qubit chips even at room temperature. Three types of Nb hydride domains are observed with varying atomic structures, crystalline orientation, and morphology, with hydrides ranging from small irregularly shaped ones (~5 nm) to large distinctly shaped (~100 nm) ones. Our findings suggest that the existence of the Nb hydride domains in Nb could be a so far unaccounted for source of the decoherence in superconducting qubits and planar Nb resonators, which may contribute to TLS and quasiparticle dissipation, as well as a source of the cooldown-to-cooldown variability and “aging”. We also identify the potential origins of the hydrogen contamination, and some promising ways of the hydride formation mitigation.

Acknowledgment

This material is based upon work supported by the U.S. Department of Energy, Office of Science, National Quantum Information Science Research Centers, Superconducting Quantum Materials and Systems Center (SQMS) under contract number DE-AC02-07CH11359.

We thank the Rigetti chip design and fabrication teams for the development and manufacturing of the qubit devices used in the reported experimental study, and for Rigetti Computing supporting the development of these devices.

We also acknowledge helpful discussions with Tiziana Spina, Lin Zhou and the valuable support and advice of cryo-TEM experiments with Charlene Wilke and Xiaobing Hu. This work made use of the EPIC, Keck-II, and/or SPID facilities of Northwestern University’s *NUANCE* Center, which received support from the Soft and Hybrid Nanotechnology Experimental (SHyNE) Resource (NSF ECCS-1542205); the MRSEC program (NSF DMR-1121262) at the Materials Research Center; the International Institute for Nanotechnology (IIN); the Keck Foundation; and the State of Illinois, through the IIN.

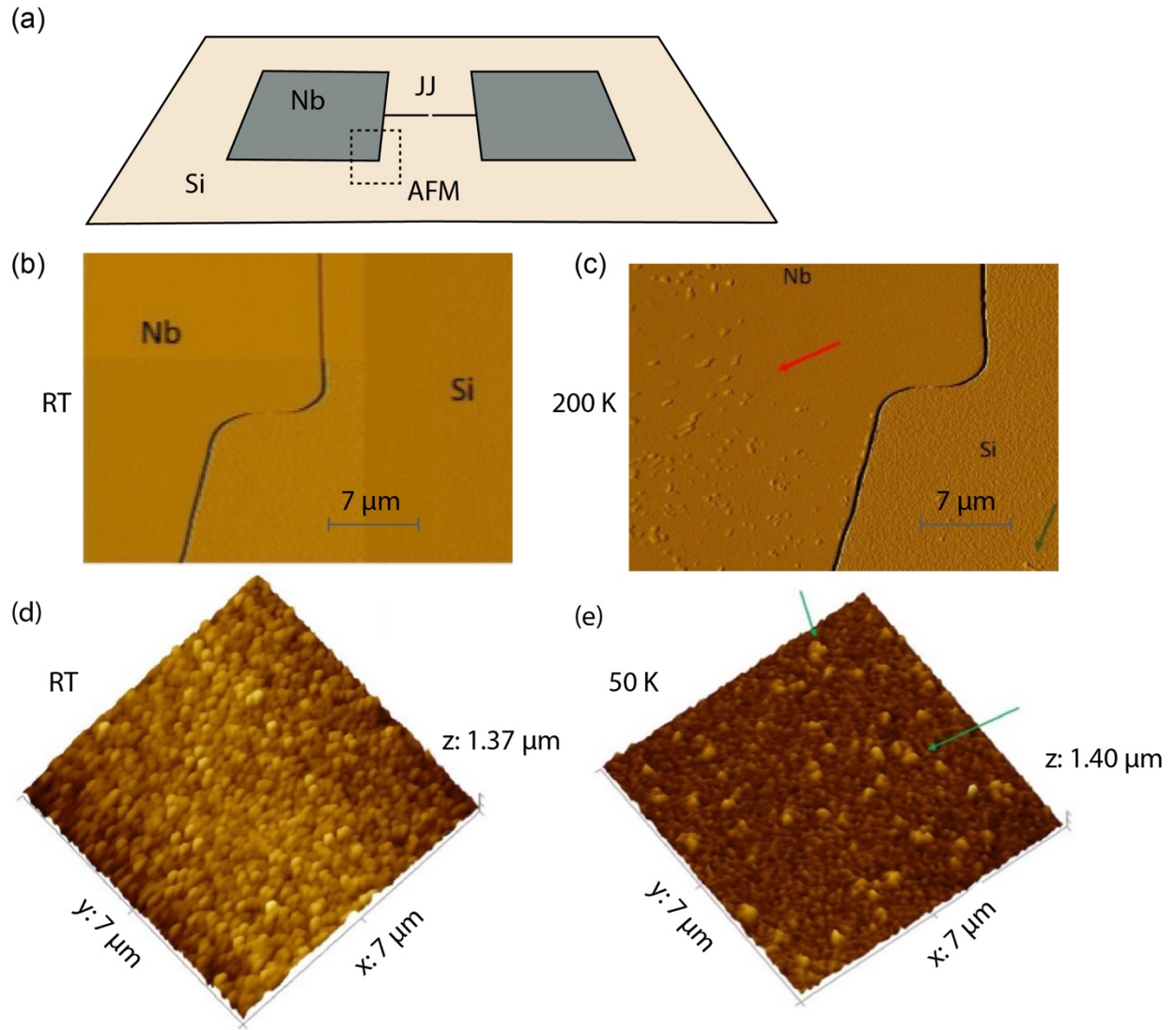


Fig. 1 (a) Schematic of the Al/AlO_x/Al Josephson junction area and cryo-AFM area of analysis; images of the surface of Nb films at (b) room temperature and (c) 200 K. Formation of unknown structures on the surface of Nb and Si is observed in cryo-AFM images. The more detailed surface topology of Nb film with further smaller scale formations is seen at (d) RT and (e) 50 K.

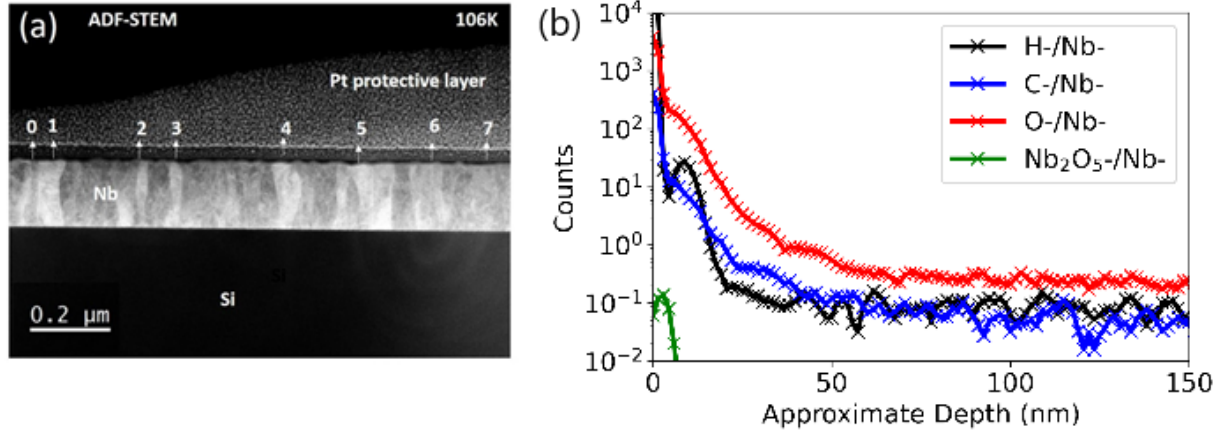


Fig. 2 (a) Annular dark-field (ADF)-STEM image of Nb/Si cross-section of Nb resonator on Si. (b) SIMS depth profiles of O, H, C impurities and the Nb₂O₅ surface oxide layer in Nb film in the transmon qubit after the fabrication process.

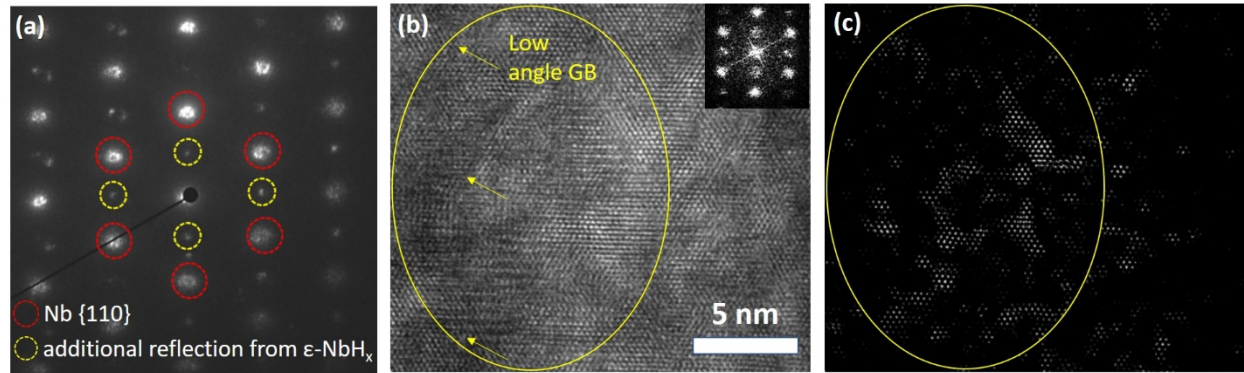


Fig. 3 (a) Nanobeam electron diffraction on a Nb grain in Fig. 2(a) shows that the additional reflections appear from ε-Nb hydride domains in the Nb grain. The orientation of ε-NbH_x (100) is parallel to Nb(110), the surface normal direction, which correspond to Type I. (b) HR-TEM image of the Nb grain with the NbH_x regions is taken at RT and shown. FFT of the HR-TEM image shows the reflections from ε-NbH_x, which agrees with the nanobeam electron diffraction pattern at 106 K. (c) Inverse filtered fast Fourier transform (FFT) image using the ε-NbH_x reflections illustrate the distribution of small ε-NbH_x precipitates in the Nb grain.

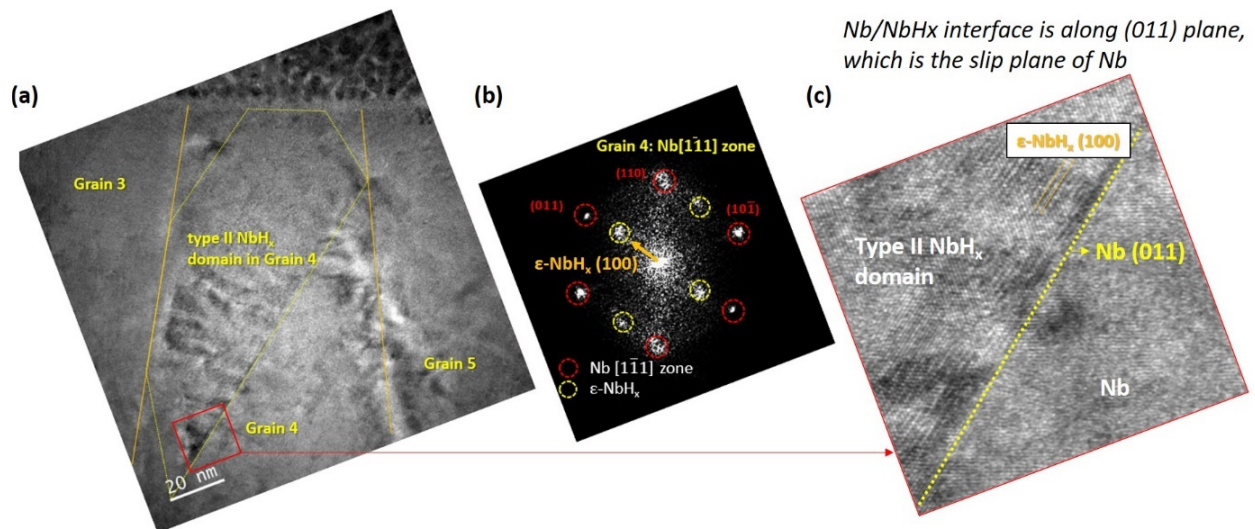


Fig. 4 HR-TEM and FFT images of Type II Nb hydride domain are illustrated. (a) Nb hydride domain is formed in the Nb grain and (b) FFT indicates that the orientation of the Nb hydride domain is Type II. (c) It is noteworthy that Nb/Nb hydride domain interface is formed along the Nb (011) plane, which is the slip plane of the BCC Nb.

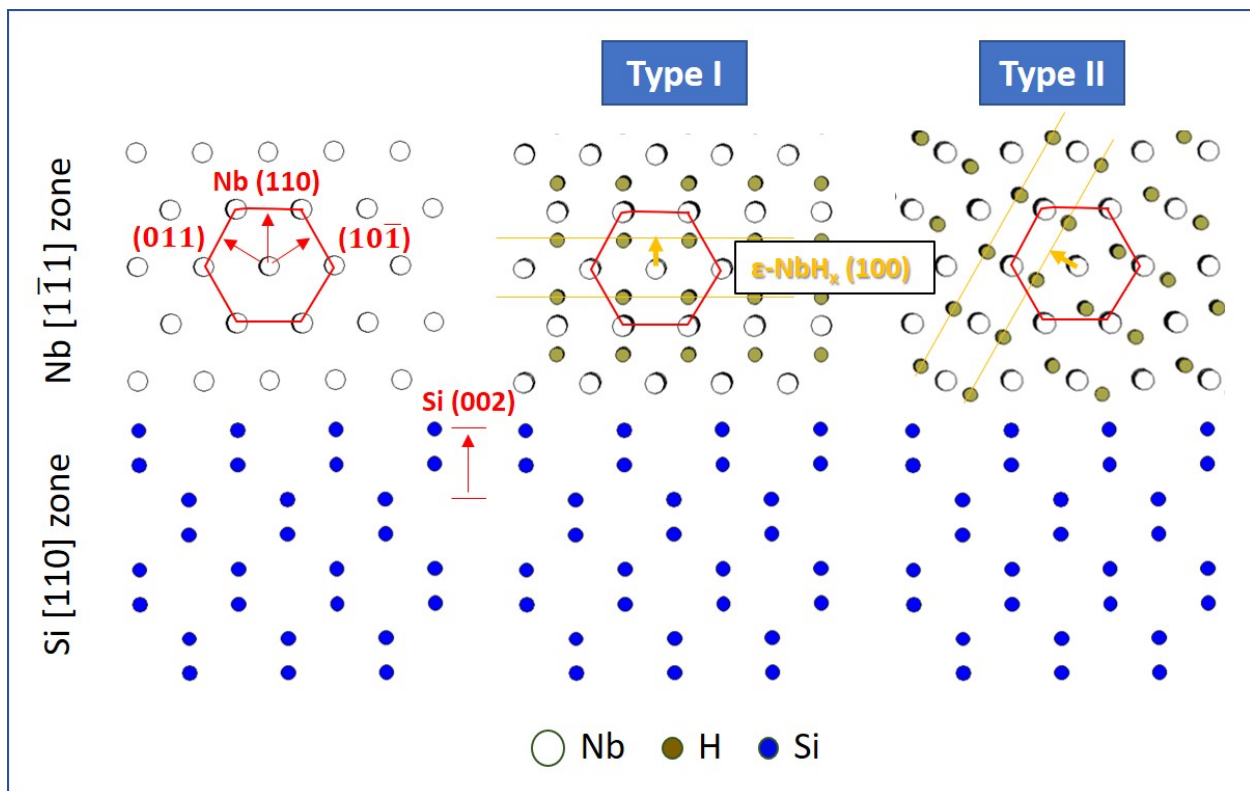


Fig. 5 Atomic arrangements of Nb hydride domain in Nb film on Si [001] substrate are illustrated. For Type I Nb hydride domains, the ϵ -NbH_x (100) plane is parallel to Nb (110), which is the surface normal plane. For Type II Nb hydride domains, ϵ -NbH_x (100) plane is parallel to Nb (011) or (10 $\bar{1}$).

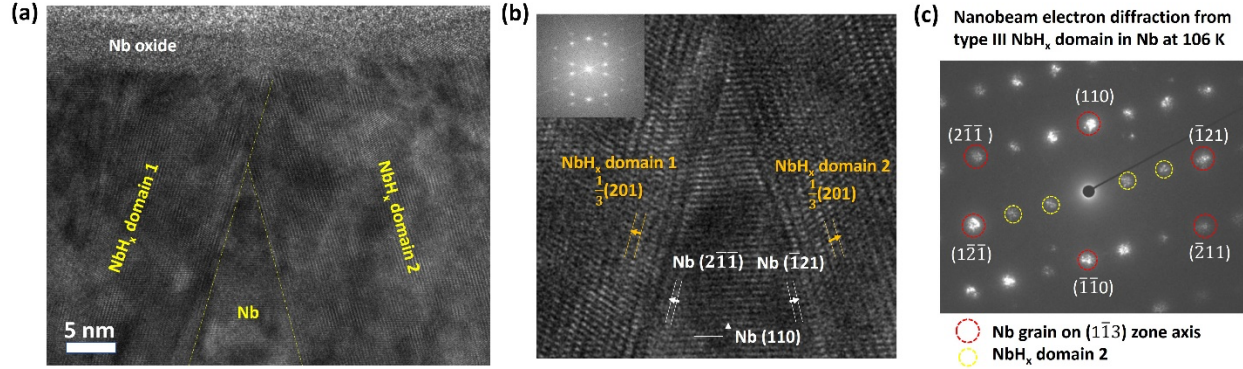


Fig. 6 (a,b) HR-TEM image of NbH_x domains in Nb grain is recorded at RT and shown. Inset in (b) is FFT of the HR-TEM image and it shows the additional reflections from the Nb hydride domain 1 and 2 (c) Nanobeam diffraction is taken on the Nb grain 7 and it displays the additional reflections from the possible NbH_x domain 2, in agreement with the HR-TEM image and FFT.

Supplementary information

Nanobeam electron diffraction is taken on the ‘domain 1’ and shows additional reflections along Nb (1 $\bar{1}$ 2) planes, indicating that additional periodicity appears along every third Nb (1 $\bar{1}$ 2) plane. Additional HR-TEM image is taken on the Nb grain no. 7, **Fig. 6(c)**, and clearly shows the two domains in the Nb grain. FFT image of the HR-TEM image also confirms that the existence of two domains in the Nb grain no. 7: domain 1 along (1 $\bar{1}$ 2) planes and domain 2 along (2 $\bar{1}\bar{1}$) planes. The simulated electron diffraction patterns of β , ϵ , ξ -Nb hydrides on Nb [131] zone axis are generated, and ϵ , ξ -Nb hydrides also show the reflections along (1 $\bar{1}$ 2) planes in the electron diffraction pattern of Nb [131] zone axis, **Fig. 6**. However, they appear every two (1 $\bar{1}$ 2) planes, which is different from every three (1 $\bar{1}$ 2) in the recorded electron diffraction pattern on the Nb grain 7 in **Fig. 3**. It may indicate that the atomic structure of Nb hydride domains 1 and 2 in grain 7 is possibly different from the ideal β , ϵ , ξ -Nb hydrides, and they are in non-equilibrium states.

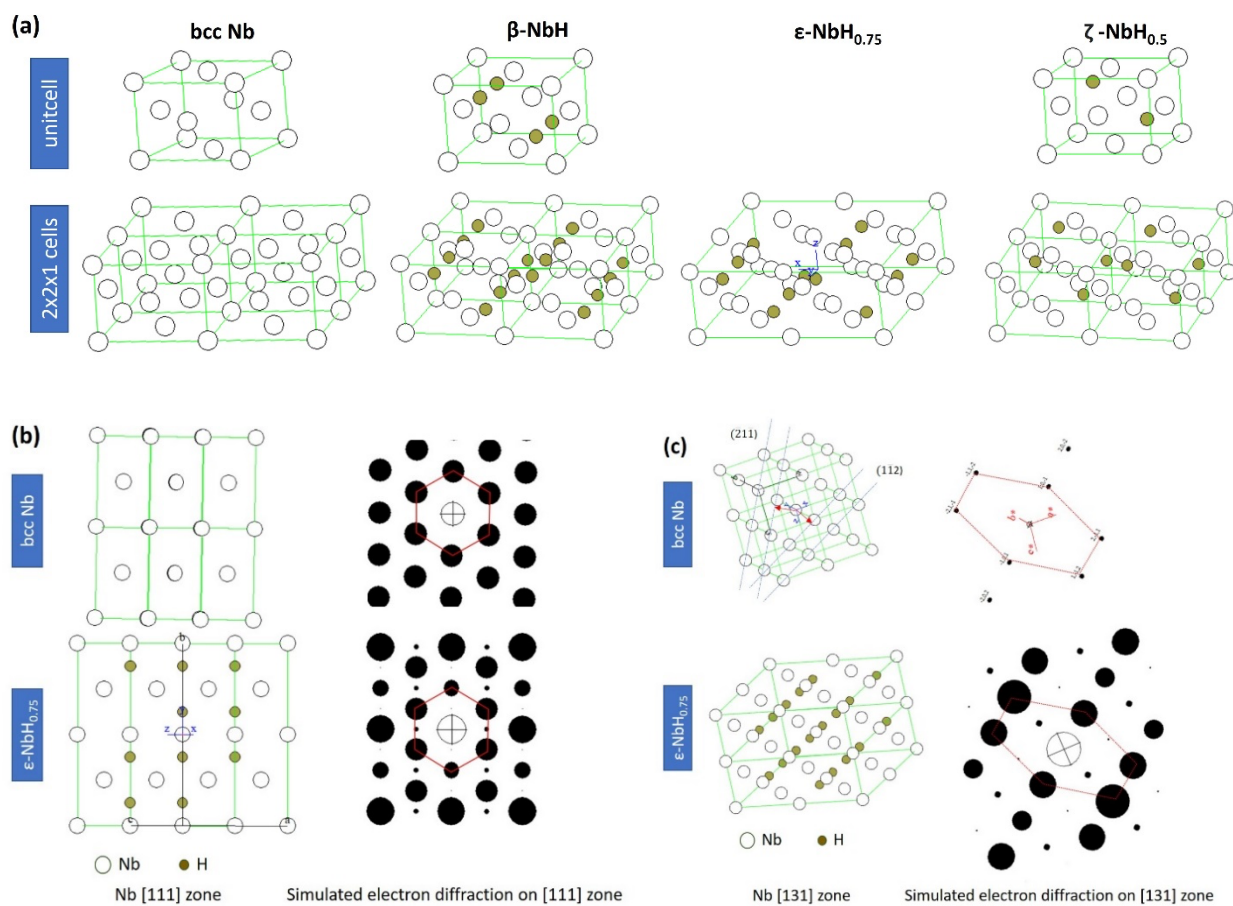


Fig. S1 (a) atomic structures of BCC Nb, Nb hydride are illustrated. Simulated electron diffraction patterns of BCC Nb and $\epsilon\text{-NbH}_{0.75}$ with different zone axis of Nb are compared: (b) Nb [111] zone axis; (c) Nb [131] zone axis.

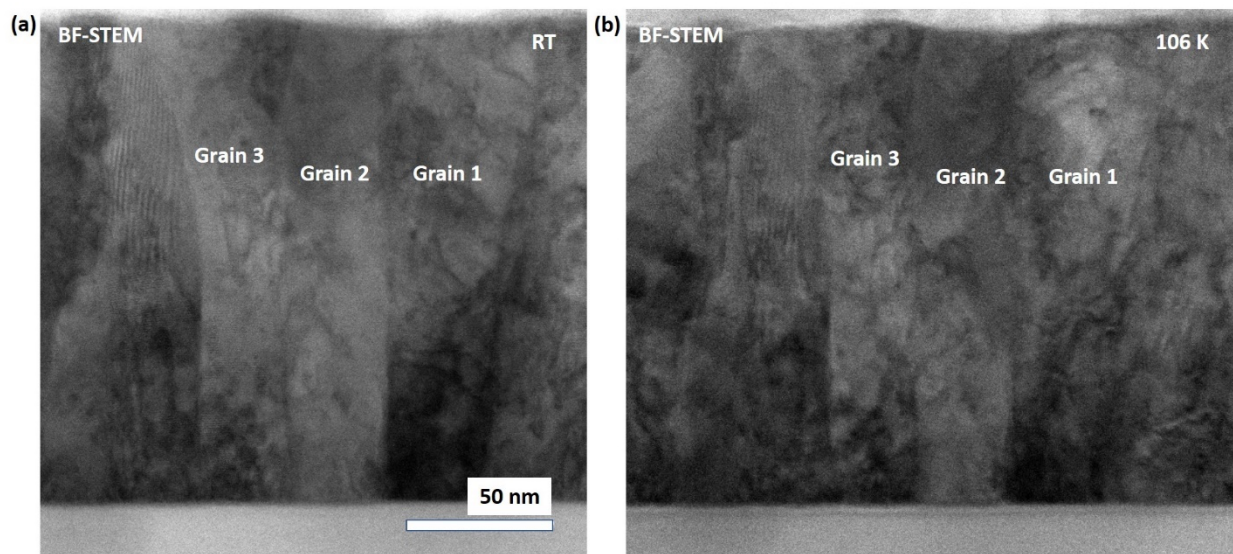


Fig. S2 BF-STEM images of Nb films, which is the same region in Fig. 1, are displayed. Grain 1 and Grain 2 contain Nb hydride domains as seen in Fig. 1. After cooling down at 106 K, there is some change in the contrast of the ADF-STEM image. Grain 1 and 2 still show similar Nb hydride domain structures at 106 K

References

- [1] C. Müller, J.H. Cole, J. Lisenfeld, Towards understanding two-level-systems in amorphous solids: insights from quantum circuits, *Rep. Prog. Phys.* 82(12) (2019) 124501.
- [2] J. Zmuidzinas, Superconducting microresonators: Physics and applications, *Annu. Rev. Condens. Matter Phys.* 3(1) (2012) 169-214.
- [3] J.M. Martinis, K.B. Cooper, R. McDermott, M. Steffen, M. Ansmann, K. Osborn, K. Cicak, S. Oh, D.P. Pappas, R.W. Simmonds, Decoherence in Josephson qubits from dielectric loss, *Phys. Rev. Lett.* 95(21) (2005) 210503.
- [4] D.P. Pappas, M.R. Vissers, D.S. Wisbey, J.S. Kline, J. Gao, Two level system loss in superconducting microwave resonators, *IEEE Transactions on Applied Superconductivity* 21(3) (2011) 871-874.
- [5] A. Premkumar, C. Weiland, S. Hwang, B. Jaeck, A.P. Place, I. Waluyo, A. Hunt, V. Bisogni, J. Pelliciari, A. Barbour, Microscopic Relaxation Channels in Materials for Superconducting Qubits, *arXiv:02908* (2020).
- [6] M. Altoé, A. Banerjee, C. Berk, A. Hajr, A. Schwartzberg, C. Song, M.A. Ghadeer, S. Aloni, M.J. Elowson, J.M. Kreikebaum, Localization and reduction of superconducting quantum coherent circuit losses, *arXiv:07604* (2020).
- [7] A. Romanenko, D. Schuster, Understanding quality factor degradation in superconducting niobium cavities at low microwave field amplitudes, *Phys. Rev. Lett.* 119(26) (2017) 264801.
- [8] A. Megrant, C. Neill, R. Barends, B. Chiaro, Y. Chen, L. Feigl, J. Kelly, E. Lucero, M. Mariantoni, P.J. O'Malley, Planar superconducting resonators with internal quality factors above one million, *Appl. Phys. Lett.* 100(11) (2012) 113510.
- [9] C.T. Earnest, J.H. Béjanin, T.G. McConkey, E.A. Peters, A. Korinek, H. Yuan, M. Mariantoni, Substrate surface engineering for high-quality silicon/aluminum superconducting resonators, *Superconductor Science Technology* 31(12) (2018) 125013.
- [10] J. Wenner, R. Barends, R. Bialczak, Y. Chen, J. Kelly, E. Lucero, M. Mariantoni, A. Megrant, P. O'Malley, D. Sank, Surface loss simulations of superconducting coplanar waveguide resonators, *Applied Physics Letters* 99(11) (2011) 113513.
- [11] A. Romanenko, R. Pilipenko, S. Zorzetti, D. Frolov, M. Awida, S. Belomestnykh, S. Posen, A. Grassellino, Three-Dimensional Superconducting Resonators at $T < 20$ mK with Photon Lifetimes up to $\tau = 2$ s, *Physical Review Applied* 13(3) (2020) 034032.
- [12] B. Makenas, H. Birnbaum, PHASE CHANGES IN THE NIOBIUM-HYDROGEN SYSTEM—II. LOW TEMPERATURE HYDRIDE PHASE TRANSITIONS, *Perspectives in Hydrogen in Metals*, Elsevier 1986, pp. 523-535.
- [13] T. Schober, H. Wenzl, The systems NbH (D), TaH (D), VH (D): Structures, phase diagrams, morphologies, methods of preparation, *Hydrogen in Metals II*, Springer 1978, pp. 11-71.
- [14] G. Rauch, R. Rose, J. Wulff, Observations on microstructure and superconductivity in the Nb-H system, *Journal of the Less Common Metals* 8(2) (1965) 99-113.
- [15] A. Nersisyan, S. Poletto, N. Alidoust, R. Manenti, R. Renzas, C.-V. Bui, K. Vu, T. Whyland, Y. Mohan, E.A. Sete, Manufacturing low dissipation superconducting quantum processors, 2019 IEEE International Electron Devices Meeting (IEDM), IEEE, 2019, pp. 31.1. 1-31.1. 4.
- [16] Y. Trenikhina, A. Romanenko, J. Kwon, J.-M. Zuo, J. Zasadzinski, Nanostructural features degrading the performance of superconducting radio frequency niobium cavities revealed by transmission electron microscopy and electron energy loss spectroscopy, *J. Appl. Phys.* 117(15) (2015) 154507.
- [17] C. Boudias, D. Monceau, *CaRIne Crystallography 3.1*, DIVERGENT SA, Centre de Transfert 60200 (1989) 1989-1998.

- [19] Y. Chang, W. Lu, J. Guérolé, L.T. Stephenson, A. Szczepaniak, P. Kontis, A.K. Ackerman, F.F. Dear, I. Mouton, X. Zhong, Ti and its alloys as examples of cryogenic focused ion beam milling of environmentally-sensitive materials, *Nature communications* 10(1) (2019) 1-10.
- [20] H. Shen, X. Zu, B. Chen, C. Huang, K. Sun, Direct observation of hydrogenation and dehydrogenation of a zirconium alloy, *J. Alloys Compd.* 659 (2016) 23-30.
- [21] D. Bafia, A. Grassellino, Z. Sung, A. Romanenko, O. Melnychuk, J. Zasadzinski, Gradients of 50 MV/m in TESLA shaped cavities via modified low temperature bake, 19th International Conference on RF Superconductivity (SRF'19), Dresden, Germany, 30 June-05 July 2019, JACOW Publishing, Geneva, Switzerland, 2019, pp. 586-591.
- [22] A. Grassellino, A. Romanenko, Y. Trenikhina, M. Checchin, M. Martinello, O. Melnychuk, S. Chandrasekaran, D. Sergatskov, S. Posen, A. Crawford, Unprecedented quality factors at accelerating gradients up to 45 MVm⁻¹ in niobium superconducting resonators via low temperature nitrogen infusion, *Supercond. Sci. Technol.* 30(9) (2017) 094004.
- [23] P. Garg, S. Balachandran, I. Adlakha, P. Lee, T. Bieler, K. Solanki, Revealing the role of nitrogen on hydride nucleation and stability in pure niobium using first-principles calculations, *Supercond. Sci. Technol.* 31(11) (2018) 115007.
- [24] Z.-H. Sung, M. Wang, A. Polyanskii, C. Santosh, S. Balachandran, C. Compton, D. Larbalestier, T. Bieler, P. Lee, Development of low angle grain boundaries in lightly deformed superconducting niobium and their influence on hydride distribution and flux perturbation, *J. Appl. Phys.* 121(19) (2017) 193903.
- [25] F. Barkov, A. Romanenko, Y. Trenikhina, and A. Grassellino. Precipitation of hydrides in high purity niobium after different treatments. *J. Appl. Phys.* **114**, 164904 (2013)
<https://doi.org/10.1063/1.4826901>
- [26] A. Grassellino, A. Romanenko, D. Sergatskov, O. Melnychuk, Y. Trenikhina, A. Crawford, A. Rowe, M. Wong, T. Khabiboulline, and F. Barkov, *Supercond. Sci. Technol.* **26**, 102001 (2013).
- [27] A. Romanenko, Y. Trenikhina, M. Martinello, D. Bafia, and A. Grassellino, in *Proceedings of the 19th International Conference on RF Superconductivity*, THP014 (2019).
- [28] K. Saito and P. Kneisel, in *Proceedings of the 5th Workshop on RF Superconductivity* (DESY, Hamburg, Germany, 1991) pp. 665–679.
- [29] A. Romanenko, F. Barkov, L. D. Cooley, A. Grassellino. Proximity breakdown of hydrides in superconducting niobium cavities. *Supercond. Sci. Technol.* **26**, 035003 (2013)
- [30] K. Serniak, M. Hays, G. de Lange, S. Diamond, S. Shankar, L. D. Burkhardt, L. Frunzio, M. Houzet, and M. H. Devoret. Hot nonequilibrium quasiparticles in transmon qubits. *Phys. Rev. Lett.* **121**, 157701 (2018)
- [31] Vepsäläinen, A.P., Karamlou, A.H., Orrell, J.L. *et al.* Impact of ionizing radiation on superconducting qubit coherence. *Nature* **584**, 551–556 (2020). <https://doi.org/10.1038/s41586-020-2619-8>
- [32] Wilen, C.D., Abdullah, S., Kurinsky, N.A. *et al.* Correlated charge noise and relaxation errors in superconducting qubits. *Nature* **594**, 369–373 (2021). <https://doi.org/10.1038/s41586-021-03557-5>
- [33] V. Chandrasekharan, R. Prozorov et al - private communication

- [34] F. Barkov, A. Romanenko, and A. Grassellino. Direct observation of hydrides formation in cavity-grade niobium. *Phys. Rev. ST Accel. Beams* **15**, 122001 (2012), <https://doi.org/10.1103/PhysRevSTAB.15.122001>
- [35] T. Higuchi, K. Saito, Y. Yamazaki, T. Ikeda, and S. Ohgushi, in *Proceedings of the 10th Workshop on RF Superconductivity* (2001), pp. 427–430.
- [36] K. Faber and H. Schultze, *Scr. Metall.* **6**, 1065 (1972).
- [37] S. Isagawa, *J. Appl. Phys.* **51**, 4460 (1980).
- [38] A. Grassellino, A. Romanenko, A. Rowe, L. D. Cooley, C. Ginsburg, and V. P. Yakovlev, in *Proceedings of IPAC'12, WEPPC115* (2012).
- [39] T. Higuchi and K. Saito, in *Proceedings of the 11th Workshop on RF Superconductivity* (2003), pp. 572–578.
- [40] Z. Sung, A. Romanenko, M. Martinello, A. Grassellino, in *Proceedings of the 19th Workshop on RF Superconductivity* (2019), TUFUB1, https://accelconf.web.cern.ch/srf2019/talks/tufub1_talk.pdf, Dresden, Germany.